AIP | APL Materials

Intrinsic nature of visible-light absorption in amorphous semiconducting oxides

Youngho Kang, Hochul Song, Ho-Hyun Nahm, Sang Ho Jeon, Youngmi Cho, and Seungwu Han

Citation: APL Materials **2**, 032108 (2014); doi: 10.1063/1.4868175
View online: http://dx.doi.org/10.1063/1.4868175
View Table of Contents: http://scitation.aip.org/content/aip/journal/aplmater/2/3?ver=pdfcov
Published by the AIP Publishing

APL MATERIALS **2**, 032108 (2014)

Intrinsic nature of visible-light absorption in amorphous semiconducting oxides

Youngho Kang,[1] Hochul Song,[1] Ho-Hyun Nahm,[2,3] Sang Ho Jeon,[4] Youngmi Cho,[4] and Seungwu Han[1,a]

[1]*Department of Materials Science and Engineering, Seoul National University, Seoul 151-755, South Korea*
[2]*Center for Correlated Electron Systems, Institute for Basic Science (IBS), Seoul 151-747, South Korea*
[3]*Department of Physics and Astronomy, Seoul National University, Seoul 151-747, South Korea*
[4]*CAE Team, Samsung Display Co., Ltd, 95 Samsung 2-ro, Giheung-gu, Youngin-City, Gyeonggi-Do 446-711, South Korea*

(Received 18 December 2013; accepted 27 February 2014; published online 17 March 2014)

To enlighten microscopic origin of visible-light absorption in transparent amorphous semiconducting oxides, the intrinsic optical property of amorphous $InGaZnO_4$ is investigated by considering dipole transitions within the quasiparticle band structure. In comparison with the crystalline $InGaZnO_4$ with the optical gap of 3.6 eV, the amorphous $InGaZnO_4$ has two distinct features developed in the band structure that contribute to significant visible-light absorption. First, the conduction bands are down-shifted by 0.55 eV mainly due to the undercoordinated In atoms, reducing the optical gap between extended states to 2.8 eV. Second, tail states formed by localized oxygen *p* orbitals are distributed over ∼0.5 eV near the valence edge, which give rise to substantial subgap absorption. The fundamental understanding on the optical property of amorphous semiconducting oxides based on underlying electronic structure will pave the way for resolving instability issues in recent display devices incorporating the semiconducting oxides. [http://dx.doi.org/10.1063/1.4868175]

The development of thin-film transistor liquid-crystal display (TFT-LCD) based on amorphous Si (*a*-Si) has brought huge impacts to the modern life by enabling large-area TVs and various mobile devices. Nevertheless, tremendous efforts are given to the next-generation display with the ultra definition, large area, and three-dimensional visual effects. The realization of such demanding performance of the display device requires high-mobility TFT components with mobility values larger than ∼20 cm^2/V s.[1,2] However, *a*-Si suffers from the low mobility below 1 cm^2/V s, and many researches are currently focused on the development of alternative materials. Among them, the transparent amorphous semiconducting oxides (TASOs) such as amorphous $InGaZnO_4$ (*a*-IGZO) are considered to be a promising contender to replace *a*-Si as the channel layer of TFTs because they are thermally stable and exhibit high electron mobility (≥10 cm^2/V s) even in the amorphous phase.[3–8] However, many studies have raised instability issues in TASO-based TFTs under various stress conditions, and this remains as a critical hurdle against the commercial application of TASOs.[9,10] In particular, negative-bias-illumination stress (NBIS) substantially shifts the threshold voltage of TFTs and it takes more than 20 h for full recovery.[11] Similarly, visible and ultra-violet (UV) light produce significant photocurrents in TASOs which last for hours or days after the light is turned off, which is called persistent photoconductivity.[9]

[a]Electronic mail: hansw@snu.ac.kr

The photoresponse of TASO is apparently at variance with optical transparency of the material, and can be attributed to the small subgap absorption which becomes substantial in the amorphous phase. The microscopic origin of the visible-light absorption is still unclear although the deep level created by the oxygen vacancy (V_O) has been suspected.[9,12] However, it is noted that the stability is mostly affected by light with the photon energy bigger than 2.6 eV, corresponding to the blue light[13] but previous theoretical works suggested based on the distribution of defect levels that the absorption by V_O occurs at light energies $\lesssim$1.9 eV.[14,15] This strongly suggests that another source of visible-light absorption may exist, possibly more intrinsic one. In this Letter, we theoretically calculate the intrinsic absorption spectrum of *a*-IGZO to identify the origin of the significant visible and near-UV light absorptions in TASOs. For the accurate comparison with experimental data, we employ GW methods to compute quasiparticle levels. In addition, several amorphous structures are generated and statistically averaged to address the structural disorder within the supercell approach. The resulting absorption spectrum agrees well with experiment and it is shown that the visible and near-UV light absorptions are caused by the tail states from the valence band and therefore is an intrinsic property of the amorphous phase.

We use Vienna *ab initio* simulation package (VASP)[16,17] for molecular dynamics (MD) simulation and electronic structure calculations. In and Ga *d* electrons are treated as frozen core electrons because their energy levels are far below than the valence band. For the exchange-correlation energy between electrons, the PBEsol functional is used during MD and relaxation steps as the functional is known to produce accurate bond lengths for many solids.[18] For calculating the density of states (DOS), the exchange-correlation functional is switched to GGA+U without further atomic relaxation.[19] In generating the amorphous structure, we apply the melt-quench method on the supercell containing 98 atoms with the composition of $InGaZnO_4$.[20,21] For comparison, we also carry out calculations on crystalline $InGaZnO_4$ (*c*-IGZO). Since the band-gap underestimation is particularly serious in this class of material, we use GW_0 methods[22] to obtain quasiparticle shifts and reflect them on the absorption coefficients.[23] The GW computational parameters such as the number of the unoccupied bands and the **k**-point mesh are determined such that the bandgap is converged within 0.1 eV. (See the supplementary material for detailed procedures.[24])

In order to consider structural fluctuations in the amorphous phase, we generate ten *a*-IGZO models through independent melt-quench processes. (Increasing the sampling number little changes the average DOS.) The averaged free energy is larger than for *c*-IGZO by 160 meV/atom, which is in good agreement with the previous theoretical study.[25] We also confirm that the structural properties such as bond lengths are similar to other theoretical works. The average DOS is obtained by aligning DOS of each model with respect to the mean oxygen 1*s* level energy within each supercell.[26] (The cell-to-cell variation is $\sim$10 meV.)

A typical atomic structure of *a*-IGZO is shown in Fig. 1(a) and it can be understood as the random packing of cation-centered polyhedra wherein the bonding configurations between metal and oxygen atoms are similar to those in the crystalline phase.[25] The pair-correlation function, $g(r)$, between metal and oxygen atoms in Fig. 1(b) confirms such structural characteristics and the bond length between a metal and first oxygen shell is almost the same as that in the crystalline phase. It is also seen that no structural ordering is found beyond the first coordination shell in *a*-IGZO. The local atomic structures such as bond lengths and coordination numbers agree reasonably with previous extended-X-ray-absorption-fine-structure (EXAFS) data for *a*-IGZO.[27,28] (See the supplementary material.[24])

To correct the band-gap underestimation in density functional theory (DFT) calculation, we carry out GW_0 calculations for five *a*-IGZO structures. The quasiparticle levels (ϵ^{QP}) with respect to GGA+U eigenvalues (ϵ^{DFT}) are provided in Fig. 2(a). It is seen that ϵ^{QP} and ϵ^{DFT} near the Fermi level follow linear relations approximately:

$$\epsilon^{QP}_{v(c)} = a_{v(c)}\epsilon^{DFT}_{v(c)} + \Delta_{v(c)}, \quad (1)$$

where $\epsilon^{QP}_{v(c)}$ is the quasiparticle energy of the valence (conduction) band. Such linear relations between quasiparticle and DFT levels were also found in other materials.[29,30] Considering the above linear relation, DOS of DFT (D^{DFT}) averaged over all the *a*-IGZO models is rescaled into DOS with GW

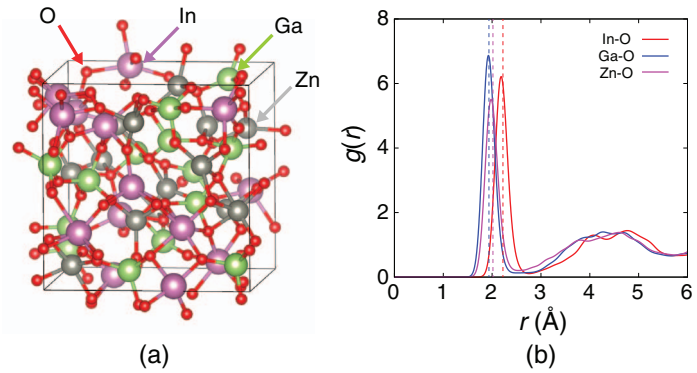

FIG. 1. (a) The amorphous structure of one of the 10 different models of *a*-IGZO. (b) Pair-correlation function between metal and oxygen atoms that is averaged over 10 models. Vertical dashed lines represent the bond length in crystalline phase.

(D^{GW}) as follows:

$$D^{GW}_{v(c)}(E) \doteq \frac{1}{a_{v(c)}} D^{\mathrm{DFT}}_{v(c)}\left(\frac{E-\Delta_{v(c)}}{a_{v(c)}}\right). \tag{2}$$

Figure 2(b) shows $D^{GW}(E)$ thus obtained.

To examine the degree of localization of each state, we evaluate inverse-participation ratios (IPRs) as shown in Fig. 2(c). The IPR is equal to $1/N$ if the state is uniformly distributed over N atoms.[31] It is noted that IPR shows clear difference between the valence and conduction band edges: the states between the Fermi level and ~ -0.5 eV are strongly localized while those near the conduction band edge are distributed broadly in spite of the structural disorder. This is because the valence band states are sensitive to the structural disorder due to the directionality of the constituent oxygen p orbitals while the conduction levels are relatively free to the disorder owing to the spherical symmetry of the metal s orbital and its unique coupling to oxygen p orbitals.[3,32] The delocalized conduction band of the amorphous $InGaZnO_4$ accounts for the high n-type conductivity of the material. Even though the strong localization of conduction tail is not observed, gradual variations in the electrostatic potential leads to fluctuation of the conduction bottom, causing slight increase of IPR near the conduction bottom. The inspection of distribution of wave functions indicates that the valence tails states, especially those near the Fermi level, are anti-bonding pairs of two close oxygen p orbitals as can be shown in the inset of Fig. 2(c).[33]

We fit DOS near the band edges using the form of $D_{v(c)}(E) \propto \sqrt{|E_{v(c)} - E|}$, where $E_{v(c)}$ represents the energy position of the mobility edge separating localized tail states from the extended states. [See dashed curves in Fig. 2(b).] It is found that E_v and E_c are -0.53 and 2.38 eV in reference to the Fermi level. Therefore, IPR and DOS fit commonly indicate the presence of tail states with the width of $\sim$0.5 and $\sim$0.1 eV in the valence and conduction bands, respectively. The large width and concentration of the tail states near the valence band edge was experimentally confirmed for amorphous zinc tin oxide.[34] The valence and conduction edges of *c*-IGZO referenced to the oxygen 1*s* level (E_v^{cryst} and E_c^{cryst}, respectively) are also marked as dashed vertical lines in Fig. 2(b). It is seen that $E_v(E_c)$ in *a*-IGZO is higher (lower) than for *c*-IGZO by 0.05 (0.55) eV, which is consistent with 0.1 (0.48) eV from XPS measurements.[35,36]

The large down-shift of conduction bottom in *a*-IGZO results in the reduction of the optical gap and should contribute to the visible-light absorption. To reveal the origin of this down-shift, we examine the electrostatic core potential (V_{core}) at the cation site using a test charge of $\sim$1 Å radii since conduction bottom states comprise mainly cation *s* orbitals. The difference from the crystalline phase, $\Delta V_{\mathrm{core}} (= V_{\mathrm{core}}^{\mathrm{amor}} - V_{\mathrm{core}}^{\mathrm{cryst}})$, is evaluated at each cation and plotted in Fig. 3(a) against the partial weight of the conduction bottom state. It is seen that the wave function is distributed mostly on cations with negative ΔV_{core}, especially In sites, and this should contribute to the energy lowering of the conduction band. In Fig. 3(b), ΔV_{core} is plotted against the coordination number (CN). The linear regression line shows that ΔV_{core} becomes lower with the reduced CN.

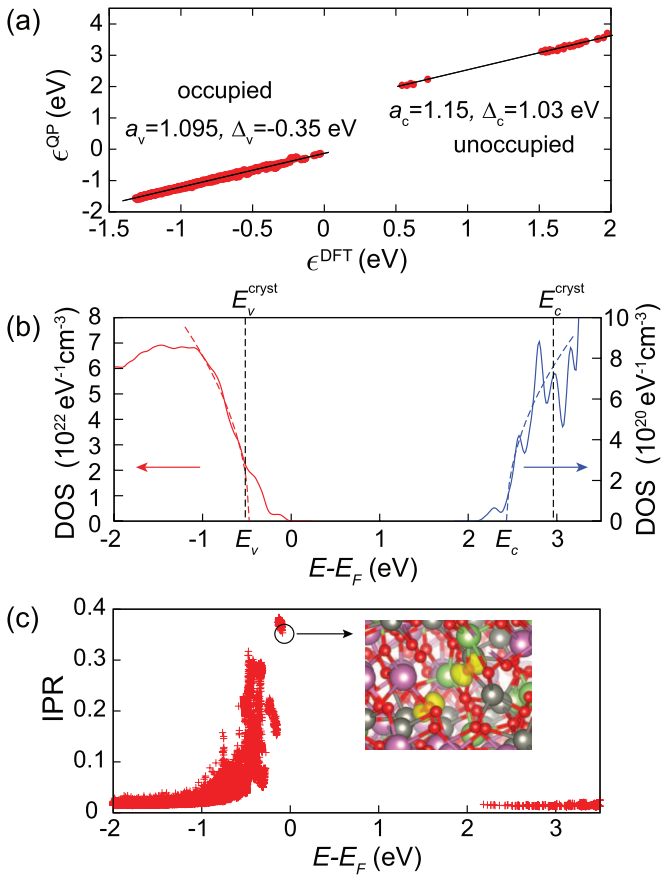

FIG. 2. (a) The quasiparticle levels (ϵ^{QP}) presented with respect to the single particle energies from GGA+U calculations (ϵ^{DFT}). The linear lines show the fitted results according to Eq. (1). (b) The density of states (DOS) of a-IGZO averaged over ten amorphous structures. The quasiparticle shift in (a) is considered by Eq. (2). The Fermi level (E_F) is set to 0. The vertical dashed lines indicate the band-edge positions of c-IGZO. (c) The inverse-participation ratio (IPR) values computed for each electronic state. The inset shows the distribution of charge density of the state at the Fermi level.

This is understandable because nearest neighbors are mostly anions and a smaller CN implies less repulsive electrostatic potential at the cation site. Therefore, the gravitation of conduction states toward undercoordinated cations mainly contribute to the reduction of optical gap in a-IGZO. In particular, the undercoordinated In atoms are most influential in lowering the conduction band, and this is consistent with the experimental finding that In-rich compounds are more prone to the instability problem.[37,38]

Next, we calculate the optical spectrum. The optical absorption coefficient (α) at the photon energy of E_{ph} is given as follows:

$$\alpha(E_{ph}) = \frac{\sqrt{2}E_{ph}}{\hbar}\left[\sqrt{\varepsilon_1^2(E_{ph}) + \varepsilon_2^2(E_{ph})} - \varepsilon_1(E_{ph})\right]^{1/2}, \quad (3)$$

where ε_1 and ε_2 are real and imaginary parts of macroscopic dielectric functions, respectively.[39] Since $\varepsilon_2/\varepsilon_1 \ll 1$ for the transition near band edges, Eq. (3) can be approximated as

$$\alpha(E_{ph}) \simeq \frac{E_{ph}}{\hbar c}\frac{\mu}{\sqrt{\varepsilon_1(0)}} JDOS(E_{ph}), \quad (4)$$

where *JDOS* represents joint density-of-states defined as

$$JDOS(E) = \int D_v(E')D_c(E'+E)dE'. \quad (5)$$

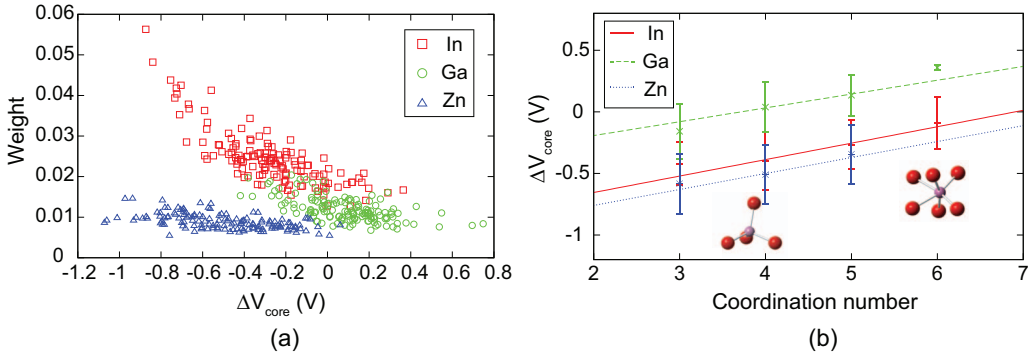

FIG. 3. (a) The partial weight of conduction bottom states on each cation plotted with respect to the difference in the electrostatic core potential between *a*- and *c*-IGZO (ΔV_{core}). (b) ΔV_{core} with respect to the coordination number (CN). The cutoff radii for counting neighboring atoms are 2.3, 2.2, and 2.1 Å for In, Zn, and Ga atoms, respectively. The straight lines are the linear regression fits. The inset figures show In atoms with distinct CNs.

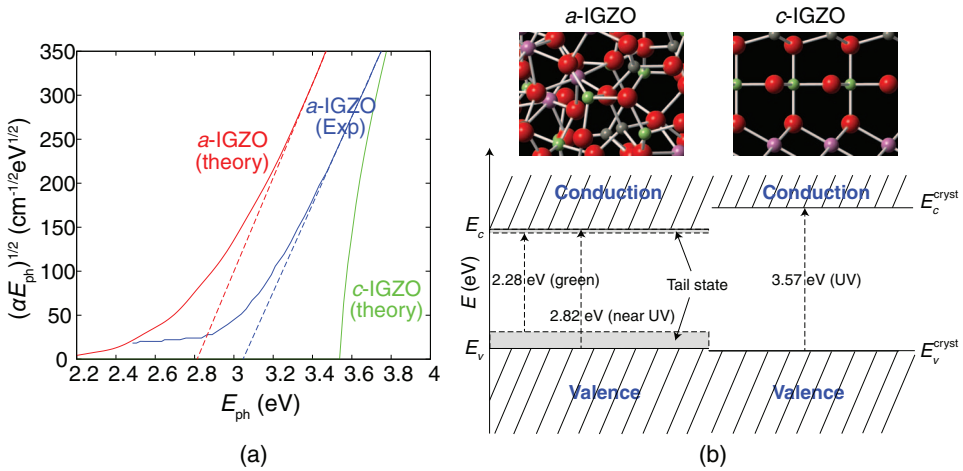

FIG. 4. Tauc plots for *a*- and *c*-IGZO calculated by Eq. (2) with quasiparticle correction and experiment.[13] The straight dashed lines indicate the linear line fitted the Tauc relation.

In Eq. (4), μ is the ratio of ε_2 to *JDOS* for the band edge transition,[40] and can be obtained by averaging *JDOS* and ε_2 over the all *a*-IGZO structures. We calculate ε_2 based on the dipole transition, and it is confirmed that the average *JDOS* rescaled with μ is in good agreement with average ε_2 (not shown).

Figure 4(a) shows the absorption coefficients presented in the form of $(\alpha E_{\rm ph})^{\frac{1}{2}}$ (so called Tauc plot). We note that DOS with *GW* correction defined by Eq. (2) is used in Eq. (5). The optical bandgap ($E_g^{\rm opt}$) is usually determined using the Tauc relation: $(\alpha E_{\rm ph})^{\frac{1}{2}} = A(E_{\rm ph} - E_g^{\rm opt})$, therefore $E_g^{\rm opt}$ is given as the extrapolated intercept at abscissa (see dashed lines). The theoretical optical gap thus obtained is 2.82 eV, which compares favorably with the experimental value of 3.05 eV.[13] In addition, we also computed $\alpha(E_{\rm ph})$ for *c*-IGZO as shown in Fig. 4(a) and the absorption edge of 3.57 eV is in good agreement with experimental value of 3.70 eV.[41]

A small discrepancy of 0.23 eV in $E_g^{\rm opt}$ of *a*-IGZO between theory and experiment could be in part attributed to the compressive strain applied on sputtered *a*-IGZO thin films because the compressive strain expands the bandgap of IGZO by increasing the overlap between metal and oxygen *s* orbitals. (Other possibilities are that the amorphous structure could be slightly different from what is modeled here or the present *GW* scheme may have some errors as in other works.[42,43]) Nonetheless, the overall profile of $\alpha(E_{\rm ph})$ near the absorption edge is similar between theory and experiment. In particular, the significant visible-light absorption above the blue region ($\geq$2.6 eV in

experiment or $\geq$2.4 eV in theory) is well reproduced in theory. It is emphasized that our amorphous models do not contain any V_O defect, and the intrinsic subgap absorption originates from the optical transition of tail states in the valence band into the conduction band. This is further supported by the fact that $E_c - E_v$ in Fig. 2(b) is 2.91 eV, close to 2.82 eV for E_g^{opt}. Figure 4(b) shows a schematic comparing the absorption behavior of *a*-IGZO and *c*-IGZO as deduced from the present computation. The finding that optical transitions from valence tail states to conduction bands are responsible for the blue to near-UV light absorption, leads us to pay attention to the peroxide formation mechanism proposed recently in Ref. 44.

The intrinsic nature of the visible-light absorption of *a*-IGZO revealed in the present work implies that there is a limitation in eliminating NBIS shift by removing defects through, say, high-pressure oxygen annealing.[45] The tail states or undercoordinated cations are intrinsic to the amorphous phase, and hence difficult to suppress unless the material composition is changed. One viable approach would be to increase the optical gap by increasing the atomic density of the amorphous film through compressive strain or dopants.

In conclusion, we theoretically investigated the optical properties of *a*-IGZO by combining GGA+U and GW_0 results. The energy levels were corrected within GW_0 method and the resulting optical spectra agree well with experiment for both crystalline and amorphous phases. Compared to *c*-IGZO, the visible-light absorption in *a*-IGZO is significantly enhanced because: (i) the conduction band energy is lowered by 0.55 eV mainly due to the undercoordinated In atoms, (ii) the localized tail states are distributed over $\sim$0.5 eV near the valence edge. The absorption of blue to near-UV light is found to occur via transitions between the valence tail states and conduction bands, which is likely to trigger the instability problem under light illumination. The fundamental understanding on the optical property of TASOs in terms of underlying band structure will pave the way for resolving the instability issues in recent display devices incorporating TASOs.

This work was supported by the Pioneer Research Center Program through the National Research Foundation of Korea funded by the Ministry of Education, Science and Technology (2012-0009563). The computations were carried out at KISTI (No. KSC-2013-C3-011).

[1] T. Kamiya, K. Nomura, and H. Hosono, Sci. Technol. Adv. Mater. **11**, 044305 (2010).
[2] H.-S. Kim, S. H. Jeon, J. S. Park, T. S. Kim, K. S. Son, J.-B. Seon, S.-J. Seo, S.-J. Kim, E. Lee, J. G. Chung, H. Lee, S. Han, M. Ryu, S. Y. Lee, and K. Kim, Sci. Rep. **3**, 1459 (2013).
[3] K. Nomura, H. Ohta, A. Takagi, T. Kamiya, M. Hirano, and H. Hosono, Nature (London) **432**, 488 (2004).
[4] H. Yabuta, M. Sano, K. Abe, T. Aiba, T. Den, and H. Kumomi, Appl. Phys. Lett. **89**, 112123 (2006).
[5] H. Q. Chiang, J. F. Wager, R. L. Hoffman, J. Jeong, and D. A. Keszler, Appl. Phys. Lett. **86**, 013503 (2005).
[6] Y. Kang, Y. Cho, and S. Han, Appl. Phys. Lett. **102**, 152104 (2013).
[7] M. P. Taylor, D. W. Readey, M. F. A. M. van Hest, C. W. Teplin, J. L. Alleman, M. S. Dabney, L. M. Gedvilas, B. M. Keyes, B. To, J. D. Perkins, and D. S. Ginley, Adv. Funct. Mater. **18**, 3169 (2008).
[8] A. J. Leenheer, J. D. Perkins, M. F. A. M. van Hest, J. J. Berry, R. P. O'Hayre, and D. S. Ginley, Phys. Rev. B **77**, 115215 (2008).
[9] S. Jeon, S.-E. Ahn, I. Song, C. J. Kim, U.-I. Chung, E. Lee, I. Yoo, A. Nathan, S. Lee, J. Robertson, and K. Kim, Nat. Mater. **11**, 301 (2012).
[10] M. D. H. Chowdhury, P. Migliorato, and J. Jang, Appl. Phys. Lett. **97**, 173506 (2010).
[11] P. Görrn, M. Lehnhardt, T. Riedl, and W. Kowalsky, Appl. Phys. Lett. **91**, 193504 (2007).
[12] B. Ryu, H.-K. Noh, E.-A. Choi, and K. J. Chang, Appl. Phys. Lett. **97**, 022108 (2010).
[13] C.-S. Chuang, T.-C. Fung, B. G. Mullins, K. Nomura, T. Kamiya, H.-P. D. Shieh, H. Hosono, and J. Kanicki, SID Int. Symp. Dig. Tech. Pap. **39**, 1215 (2008); The bandgap of the amorphous $InGaZnO_4$ depends on the growth condition, especially oxygen partial pressure, that may affect the defect density and type. Since the present study is focused on the intrinsic or stoichiometric composition, we choose this reference because the sample was grown with relatively high oxygen partial pressures and low carrier density ($\sim 10^{16}$ cm^{-3}) with additional post-annealing that may eliminate defective structures.
[14] H.-K. Noh, B. Ryu, W.-J. Lee, and K. J. Chang, Phys. Rev. B **84**, 115205 (2011).
[15] W. Körner, D. F. Urban, and C. Elsässer, J. Appl. Phys. **114**, 163704 (2013).
[16] G. Kresse and J. Furthmuller, Phys. Rev. B **54**, 11169 (1996); P. E. Blöchl, *ibid.* **50**, 17953 (1994).
[17] G. Kresse and D. Joubert, Phys. Rev. B **59**, 1758 (1999).
[18] J. P. Perdew, A. Ruzsinszky, G. I. Csonka, O. A. Vydrov, G. E. Scuseria, L. A. Constantin, X. Zhou, and K. Burke, Phys. Rev. Lett. **100**, 136406 (2008).
[19] We use U_{eff} for Zn-*d* as 7.5 eV and increase the **k**-point density to 3×3×3.
[20] The melt-quench process consists of premelting at 5000 K for 5 ps, melting at 2500 K for 10 ps, quenching to 300 K for 7.5 ps, and finally atomic positions are relaxed until the magnitudes of atomic forces are reduced below 0.02 eV/Å. The supercell lengths are fixed such that the gravimetric density corresponds to the experimental value (6.1 g/cm^3).[21] For the **k**-point sampling, we select (1/4, 1/4, 1/4) and Γ point for MD and relaxation steps, respectively.

[21] T. Kamiya, K. Nomura, and H. Hosono, J. Disp. Technol. **5**, 273 (2009).
[22] M. Shishkin, M. Marsman, and G. Kresse, Phys. Rev. Lett. **99**, 246403 (2007).
[23] The **k**-points for *GW* calculations are Γ-centered 2×2×2 and 5×5×1 **k**-point mesh grid for *a*- and *c*-IGZO, respectively. For band summation in quasiparticle shifts, 1120 and 192 bands are employed for *a*-IGZO and for *c*-IGZO, respectively.
[24] See supplementary material at http://dx.doi.org/10.1063/1.4868175 for detailed information.
[25] A. Walsh, J. L. F. D. Silva, and S.-H. Wei, Chem. Mater. **21**, 5119 (2009).
[26] L. E. Hintzsche, C. M. Fang, T. Watts, M. Marsman, G. Jordan, M. W. P. E. Lamers, A. W. Weeber, and G. Kresse, Phys. Rev. B **86**, 235204 (2012).
[27] D.-Y. Cho, J. Song, K. D. Na, C. S. Hwang, and J. H. Jeong, Appl. Phys. Lett. **94**, 112112 (2009).
[28] H. Hosono, K. Nomura, Y. Ogo, T. Uruga, and T. Kamiya, J. Non-Cryst. Solids **354**, 2796 (2008).
[29] S. Sharifzadeh, A. Biller, L. Kronik, and J. B. Neaton, Phys. Rev. B **85**, 125307 (2012).
[30] M. Rohlfing and S. G. Louie, Phys. Rev. B **62**, 4927 (2000).
[31] E. Cho, D. Kim, H. Horii, H.-S. Nam, and S. Han, J. Appl. Phys. **109**, 043705 (2011).
[32] Y. Kang, S. H. Jeon, Y. W. Son, Y. S. Lee, M. Ryu, S. Lee, and S. Han, Phys. Rev. Lett. **108**, 196404 (2012).
[33] J.-Y. Noh, H. Kim, H.-H. Nahm, D. H. Kim, B.-D. Ahn, J.-H. Lim, G. H. Kim, J.-H. Lee, J. Song, and Y.-S. Kim, J. Appl. Phys. **113**, 183706 (2013).
[34] P. T. Erslev, E. S. Sundholm, R. E. Presley, D. Hong, J. F. Wager, and J. D. Cohen, Appl. Phys. Lett. **95**, 192115 (2009).
[35] K. Lee, K. Nomura, H. Yanagi, T. Kamiya, and E. Ikenaga, J. Appl. Phys. **112**, 033713 (2012).
[36] Y. Kang, S. Lee, H. Sim, W. G. Park, S. J. Song, U. K. Kim, C. S. Hwang, S. Han, and D.-Y. Cho, "The Impact of Orbital Hybridization on the Electronic Structure of Crystalline InGaZnO: A New Perspective on the Compositional Dependence," Chem. Mater. (submitted).
[37] S. Oh, B. S. Yang, Y. J. Kim, M. S. Oh, M. Jang, H. Yang, J. K. Jeong, C. S. Hwang, and H. J. Kim, Appl. Phys. Lett. **101**, 092107 (2012).
[38] H.-S. Kim, J. S. Park, W.-J. Maeng, K. S. Son, T. S. Kim, M. Ryu, J. Lee, J. C. Lee, G. Ko, S. Im, and S. Y. Lee, IEEE Electron Device Lett. **32**, 1251 (2011).
[39] M. Gajdoš, K. Hummer, J. Furthmüller, F. Bechstedt, and G. Kresse, Phys. Rev. B **73**, 045112 (2006).
[40] B. Sadigh, P. Erhart, D. Åberg, A. Trave, E. Schwegler, and J. Bude, Phys. Rev. Lett. **106**, 027401 (2011).
[41] T. Kamiya, K. Nomura, and H. Hosono, Phys. Status Solidi A **206**, 860 (2009).
[42] M. Shishkin and G. Kresse, Phys. Rev. B **75**, 235102 (2007).
[43] C. Friedrich, M. C. Müller, and S. Blügel, Phys. Rev. B **83**, 081101 (2011).
[44] H.-H. Nahm, Y.-S. Kim, and D. H. Kim, Phys. Status Solidi B **249**, 1277 (2012).
[45] K. H. Ji, J.-I. Kim, H. Y. Jung, S. Y. Park, R. Choi, U. K. Kim, C. S. Hwang, D. Lee, H. Hwang, and K. Jeong, Appl. Phys. Lett. **98**, 103509 (2011).